Desalination and Water Treatment
www.deswater.com

doi:10.5004/dwt.2017.0623

69 (2017) 56–64
March

Modified titanate nanotubes incorporated polyamide layer for the fabrication of fouling control thin-film nanocomposite forward osmosis membranes

Rajesha Kumar*, Huda Al-Jabli, Saleh Al-Haddad, Mansour Al-Rughaib, Jasmine Samuel

Water Research Center, Kuwait Institute for Scientific Research, P.O. Box 24885, 13109 Safat, Kuwait, Tel. +965 97920482; emails: ralambi@kisr.edu.kw (R. Kumar), hjabli@kisr.edu.kw (H. Al-Jabli), shaddad@kisr.edu.kw (S. Al-Haddad), mrughaib@kisr.edu.kw (M. Al-Rughaib), jsamuvel@kisr.edu.kw (J. Samuel)

Received 3 June 2016; Accepted 23 August 2016

ABSTRACT

Titanium dioxide nanotubes (TNTs) were prepared from titanium oxide anatase powder by hydrothermal method. The hydrophilicity of TNTs was further increased by reacting with sulphuric acid to attain sulphated TNTs (STNTs) and by reacting with [(2-amino-ethyl)-3-aminopropyl] trimethoxysilane to attain amine groups (ATNTs) on TNTs surface. The additional sintering of STNTs resulted in porous crystalline structures. The thin-film nanocomposite (TFN) membranes were synthesized by incorporation of different concentrations of modified TNTs in aqueous solution of 1,3-Phenylenediamine (MPD) during the interfacial polymerization (IP) reaction with trimesoyl chloride (TMC) on polysulfone substrate. The chemical modification of TNTs was confirmed by Fourier transform infrared (FTIR) spectroscopy, and the difference in morphology of ATNTs and STNTs was determined using transmission electron microscope (TEM). The membranes morphology and their other features were studied by Field Emission Scanning Electron Microscope (FESEM), contact angle, and Atomic Force Microscope (AFM) instruments. For the fouling study, a mixture of sodium alginate and gypsum was selected as feed solution. All of the TFN membranes produced high flux and fouling resistance ratio (FRR) values than the TFC membrane. TFN-STNT membranes exhibited moderately high flux than TFN-ATNT membranes due to additional pathways for the water transport created by the porous STNTs. However, the high FRR of TFN-ATNT membranes over STNT membranes was attributed to the interaction of $–NH_2$ groups with acyl chloride groups of TMC at the outer interface during IP, results in smooth top surfaces.

Keywords: Titanium dioxide nanotubes; Forward osmosis

1. Introduction

Forward osmosis (FO) is an osmotically driven membrane process and utilizes the osmotic pressure difference across permeable membranes as driving force. Thus, to achieve high flux during the FO process, the membrane surface should be more hydrophilic; and such membranes have high tendency toward fouling during the FO-based water treatment processes [1]. Fabrication of the fouling control FO membranes is a major challenge in the large-scale optimization of the FO process in various applications. Among FO membranes, thin-film composite (TFC) membranes are potential candidates due to their high flux and easy fabrication techniques. The active layer of the TFC membrane can be tailored for hydrophilicity and smoothness for improved permeation and antifouling properties [2]. Advances in nanotechnology have led to the development of nano-structured materials, which may form the basis for novel FO membranes [3]. Many studies have demonstrated that thin-film nanocomposite (TFN) membranes can be the solution to improve not only

*Corresponding author.

Presented at the EDS conference on Desalination for the Environment: Clean Water and Energy, Rome, Italy, 22–26 May 2016.

membrane water permeability but also antifouling resistance [4,5]. Incorporating a small quantity of hydrophilic nanomaterials into a polyamide (PA) layer is apparently able to improve characteristics of PA selective layer without compromising salt separation efficiency. Inorganic nano additives like titanium dioxide (TiO_2), carbon nanotubes (CNTs), silica, silver, halloysites, and zeolite nanoparticles have contributed to improved flux and antifouling characteristics. A nano additive can improve PA film formation by offering the increased diffusion rate of monomers to the interface, increasing the hydrophilicity of the top PA surface and by reducing the roughness of the top PA surface formed [6].

Among the nanomaterials, TiO_2 nanoparticles have been used widely to improve the characteristics of membranes owing to their hydrophilicity, easy chemical modification due to available –OH groups, high chemical stability, photochemical reactivity, and potential of exhibiting antifouling nature [7,8]. Titanium dioxide nanotubes (TNTs) are another morphological form of TiO_2 nanoparticles, which can be obtained by hydrothermal method by reacting with NaOH followed by annealing. The large hydroxyl groups with specific surface area and pore volumes of TNTs, will provide abundant adsorption sites and diffusion channels for water, resulting in remarkable improvement in water productivity. The coating of nanoparticles often results in pore plugging during fabrication process causing undesirable permeability characteristics. Recently, different approaches have been developed to incorporate nanomaterials into the PA layer of TFC membrane. The entrapment of nanomaterials into the PA skin layer during interfacial polymerization (IP) is simpler and more effective when compared with the coating technique [9–11]. The other approaches include the direct binding of the nanomaterials to the membrane surface by means of covalent bonding with the amine monomer involved in IP process [12]. This approach may be advantageous as all the nanomaterials will be exposed on the surface as opposed being buried in the PA layer. The superhydrohpilic modification of the nanomaterial to attain superhydrophilic surfaces is the other method to enhance the antifouling characteristics of the TFN FO membranes [13].

The high surface energy associated with commercially available TiO_2 will result in significant particle aggregation during PA layer formation. Such agglomeration can further negatively affect the potential antifouling abilities of TiO_2 and result in surface defects in the PA layer [14]. The chemical modification of TNTs is the best strategy to minimize the chances of particle agglomeration. The presence of abundant hydroxyl groups at the TNTs surface made them readily grafted with chemical functional groups [15]. Treatment by silane coupling agents, such as 3-aminopropyltriethoxysilane (APTES), is a common approach to introduce amine functional groups on TNTs [16]. The sulphation of TiO_2 using sulphuric acid is another method to enhance its hydrophilicity [17]. The post-treatment of such sulphated TNTs (STNTs) using well-controlled sintering will exhibit different morphology compared with non-calcinated TNTs. Hou et al. reported that STNTs calcinated at 500°C are likely to possess higher surface area and crystalline porous surfaces with abundant surface hydroxyl groups and active sulphate species [18].

In the current work, TNTs were prepared by hydrothermal method from commercially available TiO_2 anatase powder. TNTs were hydrophilically modified by two different chemical reactions to attain amino groups (ATNTs) and sulphate (STNTs) groups on its surface. Further, the morphology of STNTs was altered by sintering at high temperature. The different concentrations of ATNTs and STNTs as novel fillers were incorporated into the PA layer of TFN membranes on polysulfone (PSf) substrate layer. The morphologies of two different types of membranes, and their permeability properties were determined and compared. Most of the previous studies on FO membrane fouling have focused on a single foulant. Generally, different types of organic and inorganic foulants almost always coexist in natural waters. Therefore, membranes are most likely fouled by different foulants simultaneously [19]. For example, the presence of inorganic calcium ions may accelerate organic fouling by bridging organic molecules to form a network structure in pressure-driven membrane processes [20,21]. Although FO is a non-pressure driven process, the nature of foulants present in water to be treated are the same. Thus, in the current work, the antifouling properties of the FO membranes were determined by adding a mixture of sodium alginate as organic foulant and gypsum as inorganic foulant into the feed solutions.

2. Experimental

2.1. Materials

PSf (molecular weight = 35,000 Da), polyethylene glycol (M_w = 600) as additive, [1-(2-amino-ethyl)-3-aminopropyl] trimethoxysilane (AAPTS) as silane coupling agent, and sodium alginate as foulant were purchased from Sigma-Aldrich Co. 1,3-phenylenediamine (MPD) and 1,3,5-benzenetricarbonyl trimesoyl trichloride (TMC) were the active monomers used for the synthesis of the PA selective layer and purchased from Alfa-Aesar Co. TiO_2 nanoparticles were purchased from Sigma-Aldrich Co. and used for the synthesis of titanate nanotubes (TNTs). Sodium hydroxide, hydrochloric acid, *N*-methyl pyrrolidone, *N*,*N*-dimethyl formamide, sodium chloride, gypsum ($CaSO_4$. $2H_2O$), and ethanol were purchased from Merck Co. For all FO and fouling experiments, deionized (DI) water was used.

2.2. Preparation of titania nanotubes (TNT)

50 ml of 10 M NaOH was heated to 120°C and 2 g of TiO_2 anatase powder was added in one portion, and the solution was refluxed at 120°C with continuous stirring. After 48 h of refluxing, the mixture was cooled to 30°C and poured into 500 ml of DI water. After some time, the white nanotubes settled down at the bottom of the beaker. The water layer was decanted and washing was repeated for two more times. Now 0.1 M HCl solution (150 ml) was added and the solution was stirred for 12 h at 60°C and after that, was washed again with DI water until neutral pH. Then nanotubes were centrifuged and calcinated at 450°C for 4 h.

2.3. Amination of TNT

The surface modification of TNTs was performed using silane coupling agent – AAPTS. This silane coupling agent

could be easily hydrolyzed to silanol group, and further dehydrated with surface hydroxyl groups of TNTs to produce aminated TNTs (ATNTs) [22]. In a typical experimental procedure, 2.5 g of TNTs was added to the pure ethanol (25 ml) followed by 30 min sonication in bath. A quantity of 0.5 g of AAPTS was added to the solution and stirred at 90°C for 4 h followed by filtration and subsequent washing using ethanol, ethanol/water (1:1 v/v), and water. The final products ATNTs were then dried at 100°C in a vacuum oven for 12 h.

2.4. Preparation of sulphated TNT

Sulfated-TiO_2 was synthesized as per reported literature [23]. Previously dried TNT sample was dispersed in 50 mL of isopropanol, and 2 mL of 1 M H_2SO_4 was added to the solution drop wise under stirring at 25–26°C. The solution was kept under stirring for about 4 h at the same temperature. The resulting suspension was centrifuged, washed with water, and dried in an oven at 100°C for 12 h. Further, the dry sample of STNTs was calcinated at 500°C for 5 h.

2.5. Preparation of PSf substrate layer

PSf (15.0 wt%) was taken in mixture of solvents DMF:NMP (62.25:20.75 wt%) at 26°C, and PEG (M_w = 600 Da, 2.0 wt%) was added at the same temperature. The mixture was stirred at 60°C for 4 h to obtain the homogeneous solution. The solution was degassed at 40°C for 2 h to remove the trapped air bubbles. The dope solution was poured onto a glass plate and casted by using a casting knife adjusted for the thickness of 150 µm. The glass plate was immediately immersed into a coagulation bath containing DI water at 25–26°C. After 20 min of coagulation process, the DI water was replaced with fresh water in the coagulation bath, and the membrane was allowed to stand for 24 h. Finally, the membrane was dried at 25–26°C.

2.6. Preparation of PA layer

The top active PA layer of TFN membrane was prepared by IP on the surface of a PSf substrate layer. ATNTs or STNTs in various concentrations (0.01, 0.05, and 0.1 w/v%) were dispersed in 2% (w/v) MPD aqueous solution and sonicated for 2 h at 25–26°C followed by stirring for 30 min at the same temperature to avoid nanotubes agglomeration. MPD aqueous solution was poured onto the top surface of the PSf substrate, which was held horizontally for 2 min to ensure the penetration of MPD solution into the pores of the substrate. The excess MPD solution was then drained off from the substrate surface, and a rubber roller was employed to remove the residual droplets of MPD solution. Now, 100 mL of 0.1% (w/v) TMC solution in *n*-hexane was poured onto the substrate surface. The TMC solution was drained off from the surface after 1 min contact time. After that, the TFN-FO membrane was cured at 80°C in an oven for 5 min. The unreacted MPD and TMC from the TFN membrane surface were removed by rinsing with pure *n*-hexane, and the membranes were dried at 25°C–26°C. A neat TFC membrane was prepared on the PSf substrate using the same concentrations of MPD and TMC, but without adding any TNT particles. All the prepared membranes were stored in a DI water container until they were tested. These membranes are denoted based on the wt % loading of modified TNT content in PA layer: TFN-ATNT0.01, TFN-ATNT0.05, TFN-ATNT0.1, TFN-STNT0.01, TFN-STNT0.05, TFN-STNT0.1 and TFC (control without TNTs).

2.7. Membrane characterization

The IR spectra of the modified TNTs were recorded using Cary 630 Fourier transform infrared (FTIR) instrument from Agilent technologies, USA. The spectrum was recorded in the range of 600–4000 cm^{-1} by directly placing the samples on the diamond prism followed by 32 scans. The transmission electron microscope (TEM) images of the modified TNTs were recorded using LVEM5 instrument (Delong America). The surface morphology of the membranes were recorded using Keysight 8500 Field Emission Scanning Electron Microscope (FESEM), and the imaging was conducted with back scattering electrons (BSE) mode to overcome charging effect. The surface contact angles of the membranes were recorded using optical contact angle and interface tension meter from USA KINO, model-SL200KB. The surface Atomic Force Microscope (AFM) images of the membranes were recorded using Concept Scientific Instrument (Nano-Observer), France, by scanning the membrane surface over 5 × 5 µm dimensions.

2.8. Determination of FO performance

FO experiments were conducted through a laboratory scale fabricated FO setup. It consisted of PTFE cross-flow FO cell with outer dimensions of 12.7 × 10 × 8.3 cm (Sterlitech, USA), two pumps to maintain feed and DS flow (KNF, USA), and two flow meters (Blue-White Industries). The cross-flow rates of both solutions were fixed at 8.0 cm/s, and the temperature was maintained at 25°C ± 0.5°C. The membrane coupons were inserted in the membrane cell in two different orientations: active layer facing the feed solution (AL-FS) mode and active layer facing the draw solution (AL-DS) mode. In this study, the aqueous solutions with concentrations of 2 M NaCl and 10 mM NaCl were used as draw and feed solutions, respectively. To study the impact of DS concentration on the FO performance, the high performance membrane from each series of TFN-ATNT and TFN-STNT were further subjected to flux and RSF study at two other concentrations of DS (0.5 M and 1.0 M) by maintaining the FS concentration at 10 mM NaCl. The water flux of the FO process, J (L/m^2h), was calculated from the volume changes of the IBMA-Na solutions and DI water using Eq. (1).

$$J = \frac{\Delta V}{A\Delta t} \tag{1}$$

where ΔV (L) is the volume change over a predetermined time Δt (h), and A is the effective membrane surface area (m^2).

The reverse solute flux (RSF) is a measure of the diffusion of draw solute to the feed solution during the FO

process. To determine the RSF value, the concentration of back diffused DS was measured in terms of conductivity using a calibrated conductivity meter (ORION STAR A-221 model, Thermo Scientific). The RSF, J_s (gMH), was determined using Eq. (2).

$$J_s = \frac{\Delta C_t V_t}{A\Delta t} \quad (2)$$

where C_t (g/L) and V_t (L) are the reverse solute concentration and the volume of the feed solution, respectively, at an arbitrary time t.

2.9. Fouling study of FO membranes

A 4-M NaCl solution was used as the DS in both fouling and baseline experiments. Sodium alginate and gypsum were selected as the model organic and mineral scaling agents, respectively. For baseline experiment, FS with 10 mM NaCl solution was selected with zero concentrations of both alginate and gypsum. During the fouling study, the FS consisted of 10 mM NaCl, 200 mM alginate, and 35 mM gypsum concentrations. The procedure to conduct FO membrane fouling and cleaning experiments is described as follows. First, a fresh FO membrane sample was sealed in the membrane cell with the active layer facing the feed solution (FO-mode) channel. Then, the whole membrane system was stabilized with DI water on both sides of the membrane at 25°C ± 1°C for 30 min. Baseline experiment was performed to obtain the initial membrane flux (J_{w1}) and the normalized water flux was calculated based on water flux decline. Fouling experiment was started at a cross flow rate of 0.8 L/min, pH 7.5, and temperature of 25°C ± 1°C. The permeate water was collected in the draw solution tank. The corresponding changes in the weight of draw solution were monitored, recorded, and later converted to changes in membrane flux. After the fouling experiment, the both sides of membrane sample was replaced and rinsed with fresh DI water. The cleaning experiment was carried out at higher cross flow rate (1.2 L/min) over 30 min and at temperature of 25°C ± 1°C. After membrane cleaning, baseline experiment was conducted again to determine the membrane flux (J_{w2}), and the flux recovery ratio (FRR) was calculated using Eq. (3).

$$\text{FRR}(\%) = \frac{J_{w2}}{J_{w1}} \times 100 \quad (3)$$

3. Results and discussion

3.1. Characterization of ATNTs and STNTs

3.1.1. FTIR analysis

The FTIR spectra of ATNTs and STNs are presented in Fig. 1. For STNT, a broad peak at 3,346 cm^{-1} and peak at 1,636 cm^{-1} are due to the stretching vibrations of surface hydroxyl group and adsorbed water [17]. The two peaks at 1,132 cm^{-1} and 1,044 cm^{-1} correspond to the characteristic frequencies of SO_4^{2-} [24]. The peak at 1,400 cm^{-1} is due to

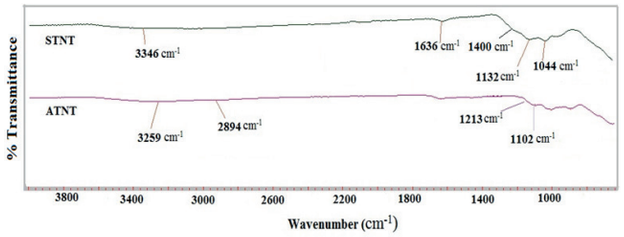

Fig. 1. FTIR spectra of ATNT and STNT.

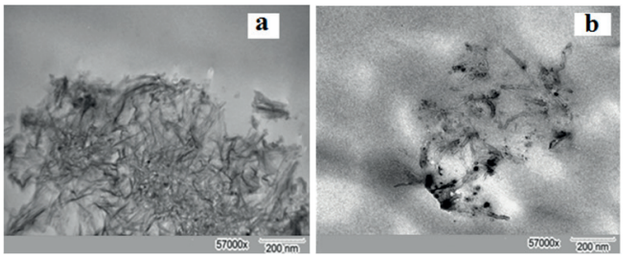

Fig. 2. TEM images of (a) ATNTs and (b) STNTs.

the stretching frequency of S-O bond. For ATNT, a broad peak around 3259 cm^{-1} is due to $-NH_2$ of ATNT merged with the peak of partly unreacted –OH groups of TNT [25]. The presence of two absorption peaks at 1,102 cm^{-1} and 1,213 cm^{-1} correspond to stretching frequencies of Si–O and C–N, respectively [26]. Meanwhile, the peak at 2,894 cm^{-1} is due to the stretching vibration of Ti–O in modified TNTs [27].

3.1.2. TEM analysis

The TEM images of ATNTs and STNTs are presented in Fig. 2. It can be clearly seen that both ATNTs and STNTs possess the shape of cylindrical tubes with a diameter in the range of 30–50 nm. However, the additional sintering of STNTs reduced the length of the tubes. The crystal size of STNTs is obviously smaller than that of ATNTs confirming that the sulphation can inhibit the growth of anatase crystallites during sintering. The sintering temperature also played a crucial role on final structures of the STNTs. The sintering at 400°C produced amorphous STNTs, while controlled sintering was performed at 500°C to obtain small crystal structures of STNTs. Such small crystal structures will lead to the formation of the pores when they are in close proximity [18].

3.2. Membrane characterization

3.2.1. Contact angle

The hydrophilicity of a membrane plays a crucial role in determining permeation and antifouling property [28]. From Fig. 3, the contact angle values of the membranes decreased with the increased loading of the modified TNTs in the PA layer. TFC membrane showed maximum contact angle value of 59°, whereas the least contact angle of 46° was observed for the TFN-STNT0.1

membrane. Thus incorporation of TNTs containing amine and sulphate groups enhanced the surface hydrophilicity of the TFN membranes. However, all TFN-STNT membranes showed relatively less contact angle values than TFN-ATNT membranes loaded with equal composition ATNTs. This small decrease in contact angle or increase in hydrophilicity may be due to the additional sintering effect of the STNTs. The additional sintering has enhanced the crystallinity of STNTs, reduced the tube length and improved porous structures on STNTs as discussed in previous section. The incorporation of such porous crystalline STNTs increased the porous structures on the PA layer there by contributing to the reduced contact angle values [29].

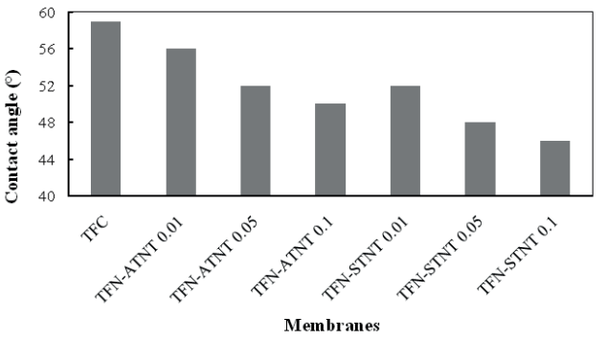

Fig. 3. Contact angle of the membranes.

3.2.2 AFM analysis

The top morphological structures of TFC, TFN-ATNT0.05, and TFN-STNT0.05 membranes were compared using 3D AFM images (Fig. 4). These changes in the roughness parameters (*Sa*, *Sq*, and *Sz*) for all TFC and TFN membranes are presented in Table 1 for better comparison. The top surfaces of all the membranes showed "ridge-and-valley" structures as typical characteristics of TFC and TFN membranes [30]. As a result of modified TNTs loading the RMS (*Sa*) values of TFN membranes increased compared with that of the TFC membrane. This indicated that the surfaces of TFN membranes are rougher compared with that of the control TFC membrane as observed by previous researchers [4,31,32]. However, the loading of STNTs resulted in rougher PA surfaces than ATNTs loading. This may be due to the interaction of $-NH_2$ groups of ATNTs with acyl chloride (–COCl) groups of TMC at the outer interface during IP reaction. Such interactions might result in additional amide linkages contributing to the smoothness of the top surface.

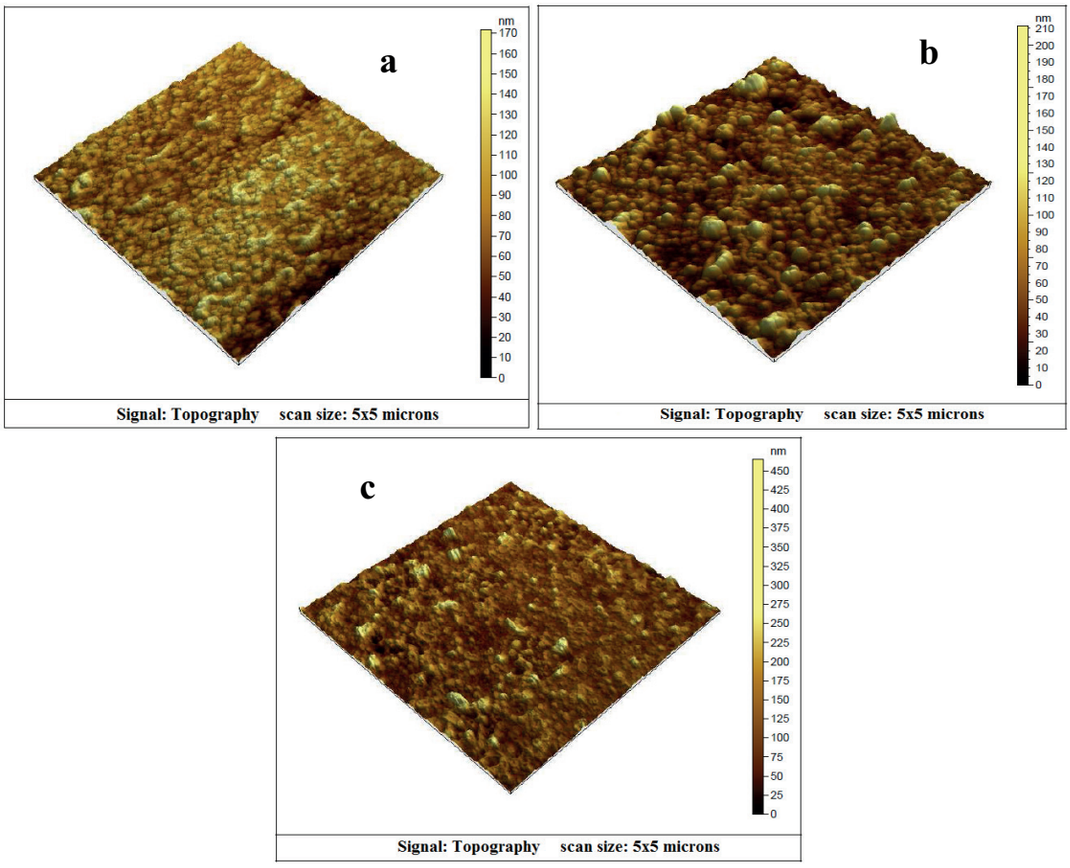

Fig. 4. AFM 3D images of the membranes; (a) TFC, (b) TFN-ATNT-0.05, and (c) TFN-STNT-0.05.

Table 1
The surface roughness parameters (*Sa*, *Sq*, *Sz*) and reverse solute flux (RSF) values of the membranes

Membrane	*Sa* (nm)	*Sq* (nm)	*Sz* (nm)	RSF (FO mode) (gMH)	RSF (PRO mode) (gMH)
TFC	17.2	21.7	172	3.4	5.0
TFN-ATNT 0.01	17.6	22.4	183	3.1	4.8
TFN-ATNT 0.05	18.0	23.8	212	2.3	4.0
TFN-ATNT 0.1	23.4	33.6	402	6.2	11.2
TFN-STNT 0.01	19.6	24.4	254	3.6	5.3
TFN-STNT 0.05	36.3	47.0	466	2.8	4.2
TFN-STNT 0.1	53.2	70.7	845	7.6	13.1

Note: For RSF, test conditions: feed solution: 10 mM NaCl, draw solution: 2.0 M NaCl, cross-flow velocity 0.8 L/min on both sides of the FO membrane, temperature: 25°C.

3.2.3 Morphology of the membrane

The surface morphology of both TFC and TFN membranes were analyzed using FESEM, and the results are presented in Fig. 5. All of the TFC and TFN membranes exhibited ridge-valley structures, which are typical characteristics of the PA layer formed by IP reaction between TMC and MPD monomers [33]. However, higher loading of the modified TNTs resulted in increased roughness of TFN membrane surfaces. This may be attributed to the promotion of IP by modified TNTs [34]. Fig. 5 (d) represents the magnified image of the TFN-STNT0.05 membrane; it indicates the formation of a porous structure on the surface, which might be contributed by the porous nature of the STNTs.

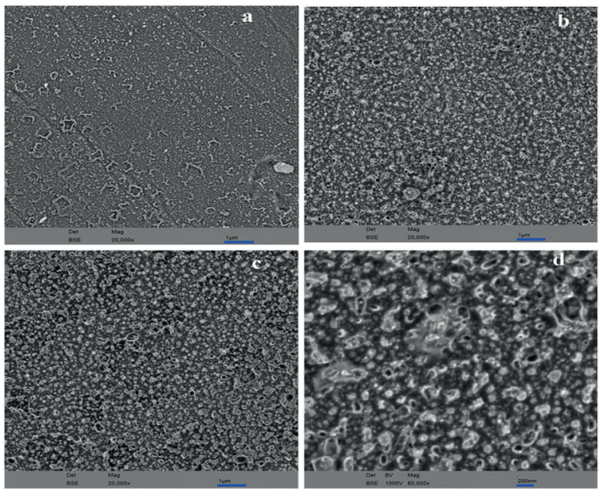

Fig. 5. FESEM images of the surfaces of (a) TFC, (b) TFN-ATNT0.05, (c) TFN-STNT0.05, and (d) magnified image of TFN-STNT0.05.

3.2.4. Membrane permeability and antifouling properties

All of the TFN membranes exhibited much higher flux compared with the TFC membrane. The higher loading of both ATNT and STNT contributed to increased permeation property of the membranes. This increased flux is due to the formation of new nano pathways created by nanotubes for the extra passage of water molecules [35]. The presence of the water channel through the hollow nanotubes and the void between the nanotubes and PA matrix contributed to the improved flux of TFN membranes. As an impact of this, the flux of TFN membranes increased with increased loading of TNTs. From Fig. 6, the TFN-STNT membranes showed moderately higher flux compared with TFN-ATNT with equal composition of nanotubes. The extra pores formed on the STNTs surfaces by sintering effect might create additional channels for the transport of water molecules. For both ATNT-TFN and STNT-TFN membranes, the maximum flux was observed when AL-DS mode. This is due to the lower internal concentration polarization of the membranes in AL-DS mode [36]. From Table 1, though the RSF of the TFN membranes is higher than the TFC membrane, the increased RSF is much lower compared with improved flux of the TFN membranes at both FO and PRO modes. For both ATNT-TFN and STNT-TFN membranes, the loading of 0.05 wt% of nanotubes termed as optimized condition for the loading of nanotubes. This composition resulted in high flux TFN membranes with relatively less RSF values. Further, the TFN membranes with 0.05 wt% of

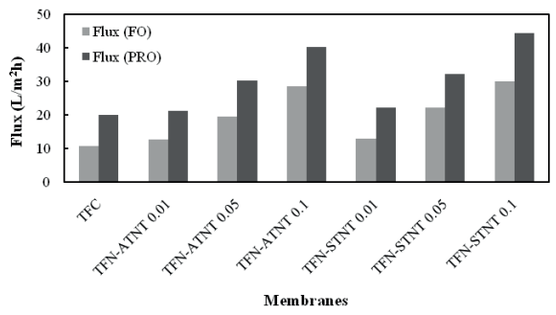

Fig. 6. Flux of the membranes at FO and PRO modes (test conditions: FS: 10 mM NaCl solution, DS: 2.0 M NaCl solution, flow rate: 0.8 L/m, temperature: 25°C).

ATNTs and STNTs exhibited relatively lower RSF values at lower concentrations of DS as presented in Table 2. Further loading of nanotubes to 0.1 wt% resulted in increased RSF values of the TFN membranes. This might be due to the lowered cross-linking degree and also enlarged microvoids

Table 2
Flux of the control TFC membrane and TFN membranes with 0.05 wt% of ATNTs and STNTs respectively at different concentrations of DS

Membranes	Flux of membranes at different DS concentrations (L/m²h)				RSF of membranes at different DS concentrations (gMH)			
	0.5 M		1.0 M		0.5 M		1.0 M	
	FO	PRO	FO	PRO	FO	PRO	FO	PRO
TFC	3.1	6.2	5.4	10.2	0.63	0.96	1.6	2.5
TFN-ATNT 0.05	4.8	7.9	10.2	15.6	0.45	0.86	0.96	1.92
TFN-STNT 0.05	5.2	8.0	11.1	16.7	0.53	0.92	1.21	2.01

Note: Test conditions: feed solution: 10 mM NaCl, cross-flow velocity 0.8 L/min on both sides of the FO membrane, temperature: 25°C.

Table 3
Comparison between the performance of the TFC FO membranes prepared in this work and TFC FO membranes reported in the literature

TFC FO membranes		Water flux (L/m²h)	Reverse salt flx (g/m²h)	Feed solution	Draw solution	Ref.
Polyamide layer	Subatrate	FO/PRO	FO/PRO			
MPD-TMC	PSf	10.8/20.1	3.4/5.0	10 mM NaCl	2 M NaCl	In this work
MPD/0.05%ATNT-TMC	PSf	19.4/30.3	2.3/4.0	10 mM NaCl	2 M NaCl	In this work
MPD/0.05%STNT-TMC	PSf	22.2/32.3	2.8/4.2	10 mM NaCl	2 M NaCl	In this work
MPD-TMC	PES	32.1/57.1	0.10/0.12	DI water	2 M NaCl	[39]
MPD-TMC	PAN	9.25/11.5	0.10/0.10	DI water	0.5 M NaCl	[40]
MPD-TMC	PES/SPSf	26.0/47.5	0.14/0.21	DI water	2 M NaCl	[41]
MPD-TMC	PES/PPSU	21.0/33.0	0.037/0.048	DI water	2 M NaCl	[42]
MPD-TMC	PES	14/32.2	0.03/0.06	DI water	0.5 M NaCl	[43]
MPD-TMC	PSf/TiO_2	29.7/56.27	0.14/0.24	10 mM NaCl	2 M NaCl	[29]
MPD/0.05%ATNT-TMC	PSf	19.0/37.0	8.8/10.2	10 mM NaCl	2 M NaCl	[34]
MPD-TMC/0.05%ATNT	PSf	20.0/32.0	2.4/4.0	10 mM NaCl	1 M NaCl	[33]
MPD/GO-TMC	PAN	33.2/55.0	12.0/14.0	DI water	2 M NaCl	[44]

Note: PES: Polyether sulfone, GO: Graphene Oxide, MPD: meta-Phenylene diamine, TMC: Trimesoyl chloride, STNT: Sulphated Titanium dioxide Nanotube, ATNT: Aminated Titanium dioxide Nanotube, SPSf: Sulphonated PSf, PPSU: Polyphenyl sulphone, PAN: Polyacrylonitrile.

between the nanotubes and polymer matrix due to excessive loading of the nanotubes. The basic performance of the TFN membranes prepared in this study and the previously reported TFC FO membranes in the literature is summarized in Table 3.

The fouling study was conducted using a mixture of sodium alginate and gypsum in the feed solution (foulant solution). Though Mi et al. reported that FO membrane flux decline due to alginate fouling is much faster in the presence of 0.5 mM calcium ions [37], in the current study 35 mM of calcium ion concentration was maintained in the foulant solution. The higher concentration of calcium ions will result in maximum bridging of alginate molecules, which eventually resulting in a dense gel layer of alginate on membrane surfaces. Also, the excess gypsum molecules present in the bulk of the solution will start adsorption and thereby initiate crystal growth on membrane surface [38]. After performing baseline experiments in FO mode, FS was replaced by the foulant solution and the fouling tests were performed in FO mode.

Fig. 7 shows the FO fouling test results for the control TFC membrane and TFN membranes with 0.05% modified

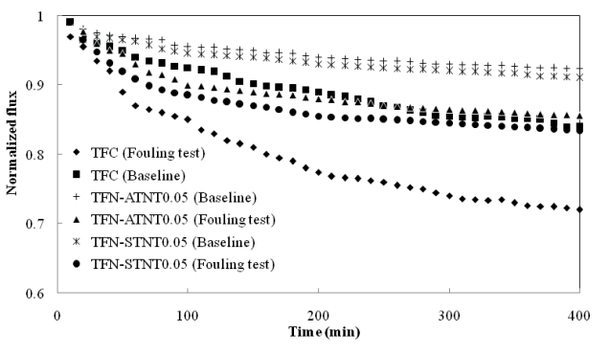

Fig. 7. Flux change versus time for the control TFC, TFN-ATNT0.05 and TFN-STNT0.05 membranes.
Note: Test conditions for the baseline experiments; 4 M NaCl draw solution and 10 mM NaCl feed solution, for fouling tests; 4 M NaCl draw solution and feed solution with mixture of 10 mM NaCl, 200 mM sodium alginate and 35 mM gypsum concentrations; the normalized flux ratio was taken with a 10-min interval during the tests.

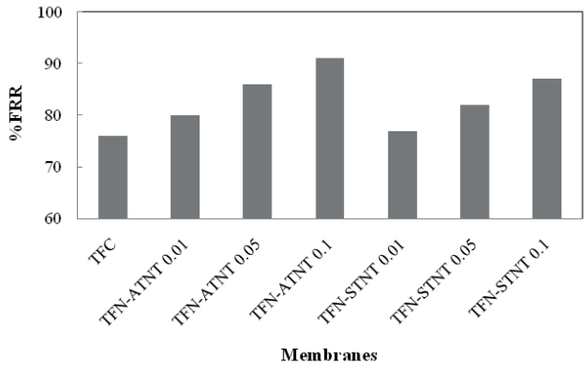

Fig. 8. The combined effect of organic and inorganic foulants on FRR values of the membranes in FO mode (test conditions: feed solution: 10 mM NaCl with 200 mg/L alginate and 1 mM gypsum, draw solution: 4.0 M NaCl, cross-flow velocity: 0.8 L/min on both sides of the FO membrane, and temperature: 25°C ± 1°C).

TNT contents. All the membranes exhibited initial flux decline during the fouling test due to severe internal concentration polarization offered by the membrane surfaces in FO mode [31]. From Fig. 7, the water flux decline of TFN membranes is much slower than that of the control TFC membrane, suggesting their lower fouling propensity. Although the foulant solution selected in the study has high tendency to bind to the membrane surface, from Fig. 8, it is worth noting that the TFN membranes showed much higher fouling resistance ratio (FRR) values than the TFC membrane. Also, it indicated that the loading of modified TNTs resulted in the easy washing of the fouled membrane surfaces. The easy cleaning of the TFN FO membranes is mainly attributed to the following reasons: (i) Most of the carboxylate groups of alginate were involved in bridging with calcium ions, the remaining functional groups of alginate, i.e., –OH groups has less affinity to bind on the membrane surfaces, which already contains $–NH_2$ (from ATNT) or $–SO_4^{2-}$ (from STNT) groups. Also, the electrostatic repulsive forces between these hydrophilic groups might have resulted in weakly binded bridged alginate molecules on the membrane surface. (ii) The increased hydrophilicity of the top PA layer of TFN membranes resulted in the formation of a hydrated layer and reduced the scaling effect by calcium ions. Also, from Fig. 7, the STNT incorporated TFN membranes showed moderately higher FRR compared with ATNT incorporated TFN membranes. This observation is in good agreement with the AFM results, as the loading of ATNT into the PA layer resulted in smooth PA surfaces when compared with the STNT loading. Such smooth surfaces reduced the sites for the deposition of Ca^{2+} ions or Ca^{2+} bridged alginate molecules.

4. Conclusions

Titania nanotubes were hydrophilically modified with amine and sulphate functional groups and successfully incorporated into a PA layer at various concentrations to obtain TFN membranes on the PSf support. The chemical modification of TNTs was confirmed by ATR-IR spectroscopy. TEM images confirmed that the additional sintering of STNTs resulted in higher crystallinity, reduced the length of the tubes and favored formation of pores on its surface compared with the non-sintered ATNTs. The FO permeation study demonstrated the higher flux of TFN-TNT membranes in both FO and PRO mode compared with neat TFC membrane. However, the TFN-STNT membranes showed moderately higher flux compared with TFN-ATNT due to porous nature of STNTs might create additional channels for the transport of water molecules. The fouling study using the mixture of alginate and gypsum at FO mode revealed that the incorporation of chemically modified TNTs into the active PA layer resulted in weak binding of calcium ion bridged alginate to the membrane surface and reduced the scaling of gypsum molecules. Such poor interaction of foulants with TFN membrane surfaces resulted in high FRR values and easy washing of membrane surfaces. The increased antifouling properties of TFN-TNT membranes compared with neat TFC membranes is due to increased hydrophilicity and surface smoothness as confirmed from contact angle and AFM studies. However, the high FRR of TFN membranes consisting of ATNTs over STNT membranes is mainly attributed to the interaction of $–NH_2$ groups of ATNTs with acyl chloride groups of TMC at the outer interface during IP, results in smooth active top surfaces.

Acknowledgements

We would like to express our gratitude to the Kuwait Institute for Scientific Research (KISR) for supporting the implementation of this research work. Furthermore, we would like to acknowledge, with much appreciation, the crucial role of the staff of the Doha Research Station of KISR, who helped us to assembling the experimental setup and gave fruitful comments and advices.

References

[1] H.B. Zhao, F. Fu, T-S. Chung, M. Weber, C. Staudt, C. Maletzko, High performance thin-film composite membranes with mesh-reinforced hydrophilic sulfonated polyphenylenesulfone (sPPSU) substrates for osmotically driven processes, J. Membr. Sci., 502 (2016) 84–93.
[2] M.A. Darwish, H.K. Abdulrahim, A.S. Hassan, A.A. Mabrouk, A.O. Sharif, The forward osmosis and desalination, Desal. Wat. Treat., 57 (2016) 4269–4295.
[3] Q. Zaib, H. Fath, Application of carbon nano-materials in desalination processes, Desal. Wat. Treat., 51 (2013) 627–636.
[4] D. Emadzadeh, W.J. Lau, T. Matsuura, M. Rahbari-Sisakht, A.F. Ismail, A novel thin film composite forward osmosis membrane prepared from PSf-TiO_2 nanocomposite substrate for water desalination, Chem. Eng. J., 237 (2014) 70–80.
[5] X. Song, Li. Wang, L. Mao, Z. Wang, Nanocomposite membrane with different carbon nanotubes location for nanofiltration and forward osmosis applications, ACS Sustain. Chem. Eng., 4 (2016) 2990–2997.
[6] A.K. Ghosh, B.-H. Jeong, X. Huang, E. Hoek, Impacts of reaction and curing conditions on polyamide composite reverse osmosis membrane properties, J. Membr. Sci., 311 (2008) 34–45.
[7] X. Cao, J. Ma, X. Shi, Z. Ren, Effect of TiO_2 nanoparticle size on the performance of PVDF membrane, Appl. Surf. Sci., 253 (2006) 2003–2010.
[8] T.-H. Bae, T.-M. Tak, Effect of TiO_2 nanoparticles on fouling mitigation of ultrafiltration membranes for activated sludge filtration, J. Membr. Sci., 249 (2005) 1–8.

[9] H.S. Lee, S.J. Im, J.H. Kim, H.J. Kim, J.P. Kim, B.R. Min, Polyamide thin-film nanofiltration membranes containing TiO_2 nanoparticles, Desalination, 219 (2008) 48–56.
[10] J. Mo, S.H. Son, J. Jegal, J. Kim, Y.H. Lee, Preparation and characterization of polyamide nanofiltration composite membranes with TiO_2 layers chemically connected to the membrane surface, J. Appl. Polym. Sci., 105 (2007) 1267–1274.
[11] S.H. Kim, S.-Y. Kwak, B.-H. Sohn, T.H. Park, Design of TiO_2 nanoparticle self- assembled aromatic polyamide thin-film-composite (TFC) membrane as an approach to solve biofouling problem, J. Membr. Sci., 211 (2003) 157–165.
[12] A. Tiraferri, C.D. Vecitis, M. Elimelech, Covalent binding of single-walled carbon nanotubes to polyamide membranes for antimicrobial surface properties, ACS Appl. Mater. Interfaces, 3 (2011) 2869–2877.
[13] A. Tiraferri, Y. Kang, E.P. Giannelis, M. Elimelech, Superhydrophilic thin-film composite forward osmosis membranes for organic fouling control: fouling behavior and antifouling mechanisms, Environ. Sci. Technol., 46 (2012) 11135–11144.
[14] A. Razmjou, J. Mansouri, V. Chen, The effects of mechanical and chemical modification of TiO_2 nanoparticles on the surface chemistry, structure and fouling performance of PES ultrafiltration membranes, J. Membr. Sci., 378 (2011) 73–84.
[15] D.V. Bavykin, F.C. Walsh, Titanate and Titania Nanotubes: Synthesis, Properties and Applications, P. O'Brien, H. Kroto, H. Craighead (Eds.) RSC Nanoscience & Nanotechnology Series, The Royal Society of Chemistry, Cambridge, 2010, chapter 4, pp. 100, 101.
[16] W.J. Lau, S. Gray, T. Matsuura, D. Emadzadeh, J.P. Chen, A.F. Ismail, A review on polyamide thin film nanocomposite (TFN) membranes: history, applications, challenges and approaches, Water Res., 80 (2015) 306–324.
[17] V.R. Pereira, A.M. Isloor, U.K. Bhat, A.F. Ismail, A. Obaid, H.K. Fun, Preparation and performance studies of polysulfone-sulfated nano-titania (S-TiO_2) nanofiltration membranes for dye removal, RSC Adv., 5 (2015) 53874–53885.
[18] Y. Hou, H. Zheng, Z. Ding, L. Wu, Effects of sintering temperature on physicochemical properties and photocatalytic activity of titanate nanotubes modified with sulfuric acid, Powder Technol., 214 (2011) 451–457.
[19] Y. Liu, B. Mi, Combined fouling of forward osmosis membranes: synergistic foulant interaction and direct observation of fouling layer formation, J. Membr. Sci., 407–408 (2012) 136–144.
[20] S. Lee, M. Elimelech, Relating organic fouling of reverse osmosis membranes to intermolecular adhesion forces, Environ. Sci. Technol., 40 (2006) 980–987.
[21] S. Lee, M. Elimelech, Salt cleaning of organic-fouled reverse osmosis membranes, Water Res., 41 (2007) 1134–1142.
[22] D. Emadzadeh, W.J. Lau, M. Rahbari-Sisakht, A. Daneshfaed, M. Ghanbari, A. Mayahi, T. Matsuura, A.F. Ismail, A novel thin film nanocomposite reverse osmosis membrane with superior anti-organic fouling affinity for water desalination, Desalination, 368 (2015) 106–113.
[23] B. Krishnakumar, M. Swaminathan, Solvent free synthesis of quinoxalines, dipyridophenazines and chalcones under microwave irradiation with sulfated Degussa titania as a novel solid acid catalyst, J. Mol. Catal. A: Chem., 350 (2011) 16–25.
[24] X. Wang, J.C. Yu, P. Liu, X. Wang, W. Su, X. Fu, Probing of photocatalytic surface sites on $SO4^{2-}/TiO_2$ solid acids by in situ FT-IR spectroscopy and pyridine adsorption, J. Photochem. Photobiol. A: Chem., 179 (2006) 339–347.
[25] L. Wang, W. Liu, T. Wang, J. Ni, Highly efficient adsorption of Cr(VI) from aqueous solutions by amino-functionalized titanate nanotubes, Chem. Eng. J., 225 (2013) 153–163.
[26] E.T. Vandenberg, L. Bertilsson, B. Liedberg, K. Uvdal, R. Erlandsson, H. Elwing, I. Lundström, Structure of 3-aminopropyl triethoxy silane on silicon oxide, J. Colloid Interface Sci., 147 (1991) 103–118.
[27] H. Niu, Y. Cai, Preparation of octadecyl and amino mixed group modified titanate nanotubes and its efficient adsorption to several ionic or ionizable organic analytes, Anal. Chem., 81 (2009) 9913–9920.
[28] R. Kumar, A.F. Ismail, Fouling control on microfiltration/ultrafiltration membranes: effects of morphology, hydrophilicity, and charge, J. Appl. Polym. Sci., 132 (2015) 1–20.
[29] F.L. Huang, Q.Q. Wang, Q.F. Wei, W.D. Gao, H.Y. Shou, S.D. Jiang, Dynamic wettability and contact angles of poly(vinylidene fluoride) nanofiber membranes grafted with acrylic acid, eXPRESS Polym. Letters, 4 (2010) 551–558.
[30] R.C. Ong, T-S. Chung, J.S. de Wit, B.J. Helmer, Novel cellulose ester substrates for high performance flat-sheet thin-film composite (TFC) forward osmosis (FO) membranes, J. Membr. Sci., 473 (2015) 63–71.
[31] D. Emadzadeh, W.J. Lau, A.F. Ismail, Synthesis of thin film nanocomposite forward osmosis membrane with enhancement in water flux without sacrificing salt rejection, Desalination, 330 (2013) 90–99.
[32] M. Ghanbari, D. Emadzadeh, W.J. Lau, T. Matsuura, M. Davoody, A.F. Ismail, Super hydrophilic TiO_2/HNT nanocomposites as a new approach for fabrication of high performance thin film nanocomposite membranes for FO application, Desalination, 371 (2015) 104–114.
[33] J. Wei, C. Qiu, C.Y. Tang, R. Wang, A.G. Fane, Synthesis and characterization of flat-sheet thin film composite forward osmosis membranes, J. Membr. Sci., 372 (2011) 292–302.
[34] G.N.B. Barona, J. Lim, M. Choi, B. Jung, Interfacial polymerization of polyamide aluminosilicate SWNT nanocomposite membranes for reverse osmosis, Desalination, 325 (2013) 138–147.
[35] D. Emadzadeh, W.J. Lau, M. Rahbari-Sisakht, H. Ilbeygi, D. Rana, T. Matsuura, A.F. Ismail, Synthesis, modification and optimization of titanate nanotubes polyamide thin film nanocomposite (TFN) membrane for forward osmosis (FO) application, Chem. Eng. J., 281 (2015) 243–251.
[36] M. Amini, A. Rahimpour, M. Jahanshahi, Forward osmosis application of modified TiO_2-polyamide thin film nanocomposite membranes, Desal. Wat. Treat., 57 (2016) 14013–14023.
[37] B. Mi, M. Elimelech, Chemical and physical aspects of organic fouling of forward osmosis membranes, J. Membr. Sci., 320 (2008) 292–302.
[38] Y. Liu, B. Mi, Effects of organic macromolecular conditioning on gypsum scaling of forward osmosis membranes, J. Membr. Sci., 450 (2014) 153–161.
[39] P. Sukitpaneenit, T.-S. Chung, High performance thin-film composite forward osmosis hollow fiber membranes with macrovoid-free and highly porous structure for sustainable water production, Environ. Sci. Technol., 46 (2012) 7358–7365.
[40] C. Klaysom, S. Hermans, A. Gahlaut, S. Van Craenenbroeck, I.F.J. Vankelecom, Polyamide/polyacrylonitrile (PA/PAN) thin film composite osmosis membranes: film optimization, characterization and performance evaluation, J. Membr. Sci., 445 (2013) 25–33.
[41] K.Y. Wang, T.S. Chung, G. Amy, Developing thin-film-composite forward osmosis membranes on the PES/SPSf substrate through interfacial polymerization, Aiche J., 58 (2012) 770–781.
[42] N. Widjojo, T.-S. Chung, M. Weber, C. Maletzko, V. Warzelhan, The role of sulphonated polymer and macrovoid-free structure in the support layer for thin-film composite (TFC) forward osmosis (FO) membranes, J. Membr. Sci., 383 (2011) 214–223.
[43] R. Wang, L. Shi, C.Y. Tang, S. Chou, C. Qiu, A.G. Fane, Characterization of novel forward osmosis hollow fiber membranes, J. Membr. Sci., 355 (2010) 158–167.
[44] L. Shen, S. Xiong, Y. Wang, Graphene oxide incorporated thin-film composite membranes for forward osmosis applications, Chem. Eng. Sci., 143 (2016) 194–205.